

# Thermal Atomic Layer Etching of Al<sub>2</sub>O<sub>3</sub> Using Sequential HF and BCl<sub>3</sub> Exposures: Evidence for Combined Ligand-Exchange and Conversion Mechanisms

Austin M. Cano, Jonathan L. Partridge, and Steven M. George\*



Cite This: *Chem. Mater.* 2022, 34, 6440–6449



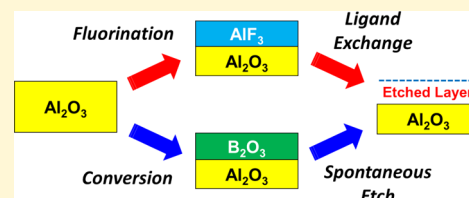
Read Online

ACCESS |

Metrics & More

Article Recommendations

**ABSTRACT:** The atomic layer etching (ALE) of Al<sub>2</sub>O<sub>3</sub> was demonstrated using sequential HF and BCl<sub>3</sub> exposures. BCl<sub>3</sub> is a new precursor for thermal Al<sub>2</sub>O<sub>3</sub> ALE that can provide pathways for both ligand-exchange and conversion etching mechanisms. Fourier transfer infrared (FTIR) spectroscopy was utilized to observe the growth of Al<sub>2</sub>O<sub>3</sub> ALD films using Al(CH<sub>3</sub>)<sub>3</sub> (trimethylaluminum) and H<sub>2</sub>O and the subsequent etching of the Al<sub>2</sub>O<sub>3</sub> ALD films using HF and BCl<sub>3</sub>. To confirm the conversion reaction, FTIR difference spectra revealed that initial BCl<sub>3</sub> exposures on the Al<sub>2</sub>O<sub>3</sub> ALD film converted the Al<sub>2</sub>O<sub>3</sub> surface to a B<sub>2</sub>O<sub>3</sub> layer. Surprisingly, larger BCl<sub>3</sub> exposures on the B<sub>2</sub>O<sub>3</sub> layer could also etch the B<sub>2</sub>O<sub>3</sub> layer. Quadrupole mass spectrometry (QMS) measurements revealed that BCl<sub>3</sub> produced ion intensities for AlCl<sub>3</sub><sup>+</sup> from AlCl<sub>3</sub> during the conversion of the Al<sub>2</sub>O<sub>3</sub> surface to a B<sub>2</sub>O<sub>3</sub> layer. Concurrently, the BCl<sub>3</sub> also etched the converted B<sub>2</sub>O<sub>3</sub> layer and ion intensities for B<sub>3</sub>O<sub>3</sub>Cl<sub>3</sub><sup>+</sup> were observed from B<sub>3</sub>O<sub>3</sub>Cl<sub>3</sub> boroxine rings. After the conversion of the Al<sub>2</sub>O<sub>3</sub> surface to a B<sub>2</sub>O<sub>3</sub> layer, the initial HF exposure then removed the B<sub>2</sub>O<sub>3</sub> layer and fluorinated the underlying Al<sub>2</sub>O<sub>3</sub> film. Following the initial BCl<sub>3</sub> and HF exposures, the FTIR difference spectra showed that Al<sub>2</sub>O<sub>3</sub> ALE proceeded primarily by a reaction pathway where HF fluorinates the Al<sub>2</sub>O<sub>3</sub> and then BCl<sub>3</sub> removes the surface fluoride layer by a ligand-exchange reaction. However, there was still evidence for some conversion of Al<sub>2</sub>O<sub>3</sub> to a B<sub>2</sub>O<sub>3</sub> layer during the subsequent BCl<sub>3</sub> exposures and then removal of the B<sub>2</sub>O<sub>3</sub> layer by the HF exposures. Spectroscopic ellipsometry measurements determined the etch rates during thermal Al<sub>2</sub>O<sub>3</sub> ALE during sequential HF and BCl<sub>3</sub> exposures. The etch rates were 0.03, 0.31, 0.65, and 0.92 Å/cycle at temperatures of 230, 255, 280, and 290 °C, respectively. QMS analysis also investigated the volatile etch products during the sequential HF and BCl<sub>3</sub> exposures on Al<sub>2</sub>O<sub>3</sub> at 270 °C. During the BCl<sub>3</sub> exposures after the initial cycle, the QMS measurements observed ion intensities for BFCl<sub>2</sub><sup>+</sup> and AlCl<sub>2</sub><sup>+</sup>. BFCl<sub>2</sub> was the major ligand-exchange product, and AlCl<sub>3</sub> was the main metal chloride etching product. In addition, small ion intensities for B<sub>3</sub>O<sub>3</sub>Cl<sub>3</sub><sup>+</sup> were also present from the conversion of Al<sub>2</sub>O<sub>3</sub> to B<sub>2</sub>O<sub>3</sub> and subsequent etching of B<sub>2</sub>O<sub>3</sub> by BCl<sub>3</sub> to yield boroxine ring products. These results indicate that thermal Al<sub>2</sub>O<sub>3</sub> ALE using sequential HF and BCl<sub>3</sub> exposures occurs by combined ligand-exchange and conversion mechanisms.



## 1. INTRODUCTION

Atomic layer etching (ALE) is a technique that can remove Ångstrom-level amounts of material using sequential surface reactions.<sup>1,2</sup> ALE can be performed using either plasma ALE or thermal ALE.<sup>1–3</sup> Both types of ALE utilize sequential surface modification and volatile release steps.<sup>1–3</sup> In plasma ALE, the volatile release is provided by energetic ions or neutral atoms through sputtering of the surface modified layer.<sup>2</sup> The sputtering can produce directional, anisotropic etching. In thermal ALE, the volatile release occurs during a chemical reaction between a gaseous reactant and the surface modified layer.<sup>1,3</sup> This gas/surface reaction is not directional and thermal ALE leads to isotropic etching.

The thermal ALE of a variety of oxide and nitride materials can be performed using sequential fluorination and ligand-exchange reactions.<sup>1,3,4</sup> The surface is first fluorinated with a fluorination agent such as HF, SF<sub>4</sub>, or XeF<sub>2</sub>.<sup>5–7</sup> This fluorination changes the oxide or nitride surface to a surface

fluoride layer. The surface fluoride layer can then be removed by various gaseous precursors through ligand-exchange reactions.<sup>1,8</sup> Other mechanisms for thermal ALE can be based on conversion reactions where the initial surface is converted to a different material that has accessible pathways for etching.<sup>9–12</sup> Conversion mechanisms are important for the thermal ALE of Si-based materials and some metals and metal oxides.<sup>9,10,13,14</sup> Other mechanisms for the thermal ALE of metals involve either oxidation or halogenation followed by ligand substitution/hydrogen transfer or ligand-addition reactions.<sup>15–18</sup>

Received: April 12, 2022

Revised: June 21, 2022

Published: July 11, 2022



The first reported thermal ALE process was  $\text{Al}_2\text{O}_3$  ALE based on sequential HF and  $\text{Sn}(\text{acac})_2$  exposures.<sup>19</sup> HF fluorinated the  $\text{Al}_2\text{O}_3$  surface, and then  $\text{Sn}(\text{acac})_2$  reacted with the fluorinated  $\text{Al}_2\text{O}_3$  surface by ligand exchange to produce volatile Al complexes.<sup>19,20</sup> These volatile Al complexes were believed to be  $\text{Al}(\text{acac})_3$ .<sup>19,20</sup> Subsequent thermal  $\text{Al}_2\text{O}_3$  ALE processes were defined using HF for fluorination and different reactants for ligand exchange. Two prominent ligand-exchange precursors have been  $\text{Al}(\text{CH}_3)_3$  and  $\text{AlCl}(\text{CH}_3)_2$ .<sup>7,21–31</sup> Mass spectrometry studies have identified the main ligand-exchange products from the  $\text{Al}(\text{CH}_3)_3$  reactant as  $\text{AlF}(\text{CH}_3)_2$  with either itself or  $\text{Al}(\text{CH}_3)_3$  in dimers or trimers.<sup>8,32</sup> Thermal  $\text{Al}_2\text{O}_3$  ALE has also been developed using  $\text{SF}_4$  for fluorination and  $\text{Sn}(\text{acac})_2$  for ligand exchange.<sup>5</sup> Other approaches for thermal  $\text{Al}_2\text{O}_3$  ALE include  $\text{NbF}_5$  for fluorination and  $\text{CCl}_4$  for ligand exchange.<sup>33</sup> Hybrid plasma/thermal  $\text{Al}_2\text{O}_3$  ALE processes have also been defined using  $\text{SF}_6$  plasma for fluorination and  $\text{Al}(\text{CH}_3)_3$  for ligand exchange.<sup>34</sup>

Although all the ligand-exchange precursors for thermal  $\text{Al}_2\text{O}_3$  ALE discussed above may etch  $\text{Al}_2\text{O}_3$ , they may not all etch other materials. These etching differences can lead to selectivity in thermal ALE.<sup>35</sup> One of the important goals for thermal ALE is to etch one material selectively in the presence of other different materials.<sup>36</sup> This goal is known as the “multiple color” challenge.<sup>36</sup> In the “multiple color” challenge, one etching process is desired to remove the “red” material and not the “blue” material. For another etching process, the objective is to remove the “blue” material and not the “red” material. The importance of thermal ALE chemistries based on different ligand-exchange precursors is to develop a portfolio of etching chemistries that can meet this “color challenge.”

Boron trichloride ( $\text{BCl}_3$ ) is a precursor that can undergo ligand exchange with metal fluorides to etch metal oxides and metal nitrides by the fluorination and ligand-exchange mechanism.  $\text{BCl}_3$  has been used previously as a ligand-exchange precursor during thermal AlN ALE using HF or  $\text{XeF}_2$  for fluorination and  $\text{BCl}_3$  for ligand exchange.<sup>37</sup>  $\text{BCl}_3$  has also been employed as a ligand-exchange precursor during thermal  $\text{TiO}_2$  ALE using  $\text{WF}_6$  for fluorination and  $\text{BCl}_3$  for ligand exchange.<sup>38</sup> In addition,  $\text{BCl}_3$  can form  $\text{B}_2\text{O}_3$  by converting the surface of a metal oxide to a  $\text{B}_2\text{O}_3$  layer and the corresponding volatile metal chloride. This conversion can occur because  $\text{B}_2\text{O}_3$  is a stable metal oxide and the conversion reaction can be thermochemically favorable. Following conversion to a  $\text{B}_2\text{O}_3$  layer, the  $\text{B}_2\text{O}_3$  can be spontaneously etched using HF exposures.<sup>10,39</sup> Spontaneous etching is chemical vapor etching as defined by continuous volatilization of material resulting from precursor exposure.<sup>39–41</sup>  $\text{BCl}_3$  was used previously during  $\text{WO}_3$  thermal ALE for the conversion of the surface of  $\text{WO}_3$  to a  $\text{B}_2\text{O}_3$  layer.<sup>10</sup> The  $\text{B}_2\text{O}_3$  layer was then removed by spontaneous etching resulting from HF exposures.<sup>10</sup>

This study explored thermal  $\text{Al}_2\text{O}_3$  ALE using sequential exposures of HF and  $\text{BCl}_3$ . The key question was the reaction mechanism. Will  $\text{Al}_2\text{O}_3$  be etched by a fluorination and ligand-exchange mechanism as illustrated in Figure 1? Or will  $\text{Al}_2\text{O}_3$  be etched by conversion to  $\text{B}_2\text{O}_3$  by  $\text{BCl}_3$  followed by the spontaneous etching of  $\text{B}_2\text{O}_3$  by HF as displayed in Figure 2? To investigate thermal  $\text{Al}_2\text{O}_3$  ALE and discover the reaction mechanism, in situ Fourier transform infrared (FTIR) spectroscopy was used to monitor the surface compositional changes during sequential HF and  $\text{BCl}_3$  exposures. In situ quadrupole mass spectrometry (QMS) analysis was also utilized to monitor the volatile etch products formed during

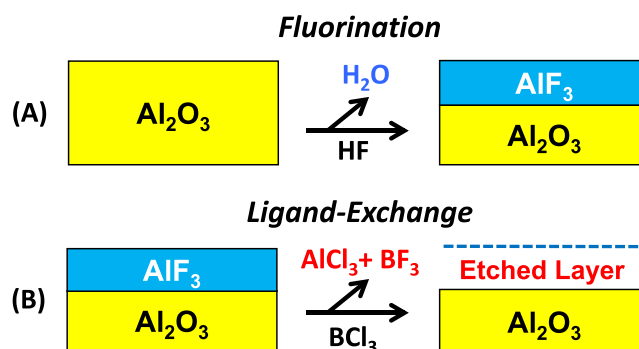


**Figure 1.** Thermal  $\text{Al}_2\text{O}_3$  ALE occurring by a fluorination and ligand-exchange mechanism. (A) HF fluorinates  $\text{Al}_2\text{O}_3$  to produce  $\text{AlF}_3$  and gaseous  $\text{H}_2\text{O}$ . (B)  $\text{BCl}_3$  then undergoes a ligand-exchange reaction with  $\text{AlF}_3$  to remove the  $\text{AlF}_3$  layer by producing gaseous  $\text{AlCl}_3$  and  $\text{BF}_3$ .

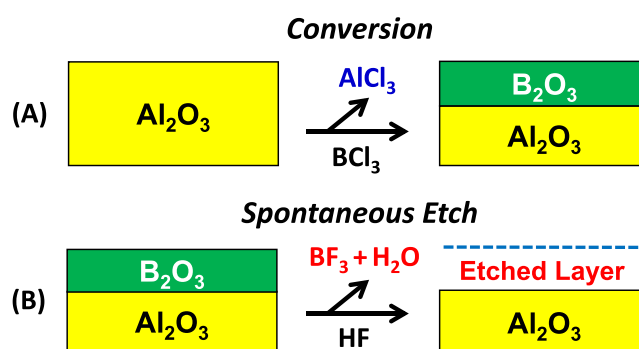


**Figure 2.** Thermal  $\text{Al}_2\text{O}_3$  ALE occurring by a conversion and spontaneous etch mechanism. (A)  $\text{BCl}_3$  converts  $\text{Al}_2\text{O}_3$  to  $\text{B}_2\text{O}_3$  and gaseous  $\text{AlCl}_3$ . (B) HF then spontaneously etches the  $\text{B}_2\text{O}_3$  layer by producing gaseous  $\text{BF}_3$  and  $\text{H}_2\text{O}$ .

the sequential HF and  $\text{BCl}_3$  exposures. In addition, in situ spectroscopic ellipsometry studies were performed to measure  $\text{Al}_2\text{O}_3$  film thicknesses during the ALE cycles to determine  $\text{Al}_2\text{O}_3$  etch rates.

## 2. EXPERIMENTAL METHODS

The in situ FTIR spectroscopy studies were performed in a warm-walled viscous flow reactor as described earlier.<sup>20,42</sup> The reactor was heated by a custom ceramic heater (Watlow). The wall temperature was held at 150 °C during both the ALD and ALE experiments. To enhance the surface sensitivity, the FTIR experiments were performed in transmission mode through high surface area silicon nanoparticles.<sup>9</sup> The silicon nanoparticles had an average diameter of 30–50 nanometers (US Research Nanomaterials). The use of nanoparticles to facilitate FTIR vibrational spectroscopy studies of surface processes has been discussed earlier.<sup>43,44</sup>

For the transmission FTIR measurements, the silicon nanoparticles were pressed into a tungsten grid with dimensions of 3 cm by 1.7 cm with a thickness of 50  $\mu\text{m}$  and 100 gridlines per in.<sup>43</sup> The grid had tantalum foils spot-welded on each side of the grid to provide good electrical contact for resistive heating. To increase the temperature, the tungsten grid was resistively heated by a direct current power supply (HP 6268B). This current was regulated using a temperature controller (16B PID Love). To monitor the temperature, a type-K thermocouple was attached to the tungsten grid with an insulating epoxy (Ceramaxbond, Aremco 571).

The FTIR spectra were recorded using a Nicolet 6700 spectrometer with a KBr beam splitter. The infrared light was generated from a glow bar light source. The light was directed outside the spectrometer, entered the reactor through a KBr window, passed

through the tungsten grid containing the silicon nanoparticles, exited the reactor through another KBr window, and was then focused onto an MCT-B detector. The two KBr windows were isolated from the reactor by gate valves. These gate valves were only opened when obtaining the FTIR spectra. The FTIR spectra were averaged for 100 scans with a resolution of  $4\text{ cm}^{-1}$ . Background reference spectra were collected before each experiment.

The  $\text{Al}_2\text{O}_3$  ALD was performed in the in situ FTIR reactor using trimethylaluminum (TMA) (Sigma-Aldrich, 99.5%) and reagent-grade water ( $\text{H}_2\text{O}$ , Sigma). The  $\text{Al}_2\text{O}_3$  ALD was conducted at  $200\text{ }^\circ\text{C}$  and employed TMA exposures at 100 mTorr for 1 s and  $\text{H}_2\text{O}$  exposures at 70 mTorr for 2 s. The  $\text{Al}_2\text{O}_3$  ALE studies were performed using HF-pyridine (70% HF, 30% pyridine, Millipore-Sigma) as the fluorination reactant together with  $\text{BCl}_3$  (Synquest Chemicals, 99%). The HF-pyridine solution has an HF vapor pressure of 90–100 Torr with negligible pyridine vapor pressure at room temperature.<sup>45,46</sup> These ALE investigations were performed at  $300\text{ }^\circ\text{C}$  and utilized HF exposures at 200 mTorr for 1 s and  $\text{BCl}_3$  exposures at 500 mTorr for 1 s. The HF-pyridine was transferred to a stainless-steel bubbler that was gold-plated to prevent corrosion of the stainless-steel walls. A carrier gas of UHP  $\text{N}_2$  flowed through the FTIR reactor at a flow rate of 100 sccm. This  $\text{N}_2$  gas flow established a background  $\text{N}_2$  pressure of 1.5 Torr in the reactor.

The in situ spectroscopic ellipsometry studies of ALD and ALE were conducted in a second reactor that has been described previously.<sup>10</sup> This reactor is a warm-walled reactor with a heated sample holder that achieved temperatures up to  $300\text{ }^\circ\text{C}$ . The polarized light from the ellipsometer was incident on the sample surface at a  $70^\circ$  angle from the surface normal. A spectroscopic ellipsometer (M-2000, J. A. Woollam) was utilized for all ellipsometry experiments. Wavelengths from 240 to 1700 nm were used to obtain the film optical properties. The  $\Psi$  and  $\Delta$  parameters were analyzed using a software package (CompleteEASE, J. A. Woollam). Silicon coupons with a native oxide were used as the substrates for  $\text{Al}_2\text{O}_3$  ALD. A Cody Lorentz model was used to fit the data during  $\text{Al}_2\text{O}_3$  ALD. The  $\text{Al}_2\text{O}_3$  ALD films were grown using TMA and ozone from an ozone generator (Ozonia).

QMS was performed in a reactor that has been described previously.<sup>3</sup> The reactants were exposed to  $\text{Al}_2\text{O}_3$  and  $\text{B}_2\text{O}_3$  powders (US Research Nanomaterials). The volatile etch products were formed in a  $\text{N}_2$  background gas at a pressure of  $\sim 4.5$  Torr in the sample holder. These gases expanded through an aperture into a low pressure differentially pumped region to form a molecular beam. The products in the beam then passed through a skimmer into a second differentially pumped region that housed the quadrupole mass spectrometer (Extrel, MAX-QMS Flanged Mounted System). An electron ionization energy of 70 eV was used for the QMS experiments. To minimize exposures to corrosive gases, the ionizer and analyzer were positioned perpendicular to the incoming molecular beam.

### 3. RESULTS AND DISCUSSION

**3.1. FTIR Studies of  $\text{Al}_2\text{O}_3$  ALD,  $\text{Al}_2\text{O}_3$  ALE, and  $\text{Al}_2\text{O}_3$  Conversion to  $\text{B}_2\text{O}_3$ .** Figure 3 shows the growth of an  $\text{Al}_2\text{O}_3$  ALD film on the silicon nanoparticles as measured by FTIR spectroscopy. The  $\text{Al}_2\text{O}_3$  ALD was conducted at  $200\text{ }^\circ\text{C}$  using sequential exposures of TMA and  $\text{H}_2\text{O}$ . One ALD cycle was defined by one TMA exposure followed by one  $\text{H}_2\text{O}$  exposure. The spectra in Figure 3 display the absorbance growth from the Al–O stretching mode at  $850\text{ cm}^{-1}$ .<sup>21,43</sup> The absorbance for this vibrational mode increases with increasing number of ALD cycles during the nine ALD cycles. The spectra were all recorded after the  $\text{H}_2\text{O}$  exposures. The additional small absorption peak at  $1130\text{ cm}^{-1}$  is assigned to a Si–O–Al vibrational mode. The Si–O–Al species is formed during the initial stages of  $\text{Al}_2\text{O}_3$  ALD at the interface with the native oxide film on the silicon nanoparticles. After the TMA exposures (not shown), the absorption peak observed at

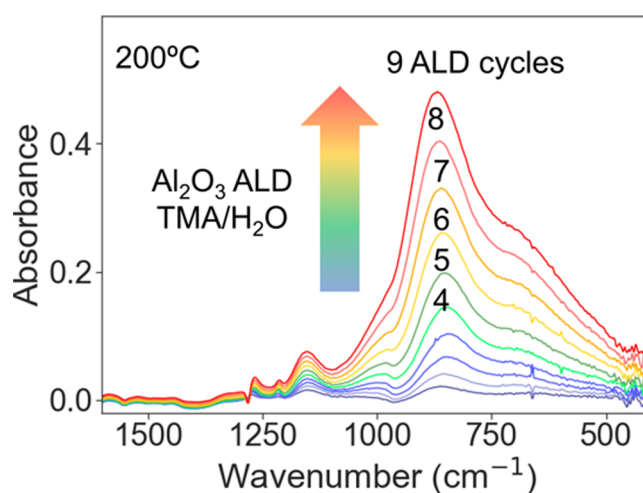


**Figure 3.** FTIR spectra of growth of  $\text{Al}_2\text{O}_3$  ALD films on silicon nanoparticles during first 9  $\text{Al}_2\text{O}_3$  ALD cycles using TMA and  $\text{H}_2\text{O}$  as reactants at  $200\text{ }^\circ\text{C}$ . Spectra show progressive absorbance gain of Al–O vibrations. Spectra were recorded after  $\text{H}_2\text{O}$  exposures.

$1215\text{ cm}^{-1}$  was assigned to Al– $\text{CH}_3$  deformation modes from Al– $\text{CH}_3$  species.<sup>7,22</sup> In addition, the absorption peak monitored at  $2900\text{ cm}^{-1}$  was attributed to C–H stretching vibrations from surface Al– $\text{CH}_3$  species.<sup>7,22</sup>

Figure 4 shows the etching of the  $\text{Al}_2\text{O}_3$  ALD film by thermal  $\text{Al}_2\text{O}_3$  ALE using sequential exposures of HF and  $\text{BCl}_3$

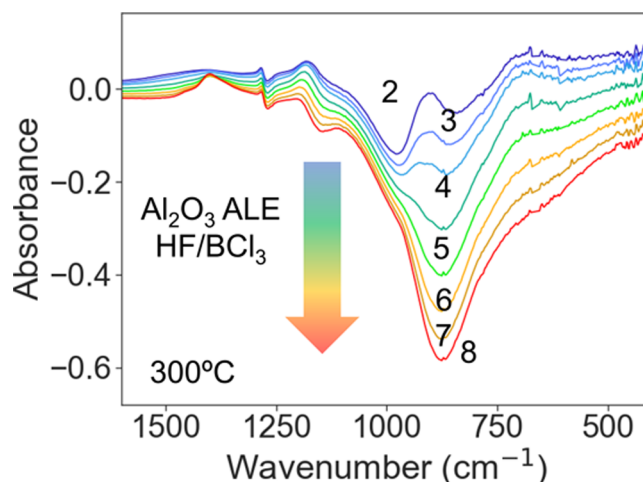


**Figure 4.** FTIR spectra of etching of  $\text{Al}_2\text{O}_3$  ALD films during first 8  $\text{Al}_2\text{O}_3$  ALE cycles using HF and  $\text{BCl}_3$  as reactants at  $300\text{ }^\circ\text{C}$ . Spectra show progressive absorbance loss of Al–O vibrations. Spectra were recorded after  $\text{BCl}_3$  exposures.

at  $300\text{ }^\circ\text{C}$ . Figure 4 displays difference spectra referenced to the initial  $\text{Al}_2\text{O}_3$  ALD film. There is clear evidence of  $\text{Al}_2\text{O}_3$  etching because the absorbance from the Al–O vibrational band at  $850\text{ cm}^{-1}$  decreases progressively during the 8  $\text{Al}_2\text{O}_3$  ALE cycles. The spectra were all recorded after the  $\text{BCl}_3$  exposures. The difference spectra in Figure 4 also display a small increase in absorbance at  $1370\text{ cm}^{-1}$  attributed to a B–O vibrational mode.<sup>39</sup> The appearance of this B–O vibrational mode may indicate that  $\text{BCl}_3$  can convert  $\text{Al}_2\text{O}_3$  to  $\text{B}_2\text{O}_3$  by the reaction  $\text{Al}_2\text{O}_3 + 2\text{BCl}_3(\text{g}) \rightarrow \text{B}_2\text{O}_3 + 2\text{AlCl}_3(\text{g})$ , as shown in Figure 2.<sup>10,11</sup> Thermochemical calculations yield a small positive standard free energy change of  $\Delta G^0 = +2.3\text{ kcal/mol}$

for this reaction at 300 °C.<sup>47</sup> Although  $\Delta G^0$  is slightly positive, this conversion could be feasible under the nonstandard and nonequilibrium conditions for this surface reaction.

To explore the possibility that  $\text{BCl}_3$  can convert  $\text{Al}_2\text{O}_3$  to  $\text{B}_2\text{O}_3$ , difference spectra were recorded during successive  $\text{BCl}_3$  exposures on an  $\text{Al}_2\text{O}_3$  ALD film. Figure 5 shows the difference

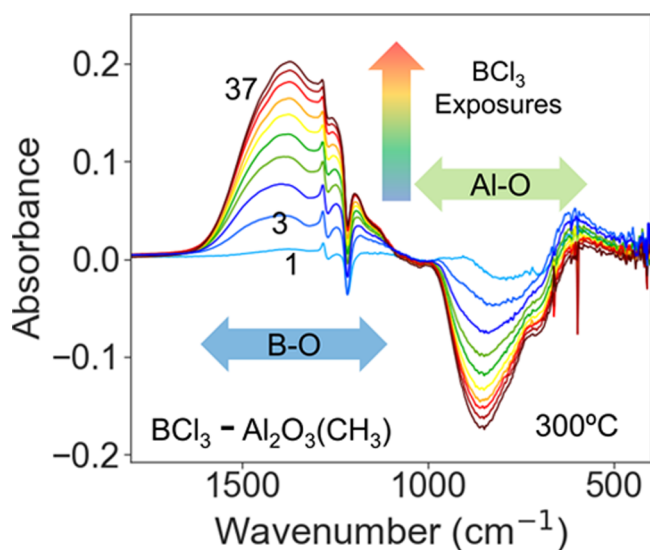


**Figure 5.** FTIR difference spectra showing conversion of  $\text{Al}_2\text{O}_3$  ALD films to  $\text{B}_2\text{O}_3$  using 37  $\text{BCl}_3$  exposures at 300 °C. Spectra display absorbance loss of Al–O vibrations for  $\text{Al}_2\text{O}_3$  and absorbance gain of B–O vibrations for  $\text{B}_2\text{O}_3$ . Difference spectra are referenced to a methyl-terminated  $\text{Al}_2\text{O}_3$  ALD film after TMA exposure.

spectra corresponding to 37  $\text{BCl}_3$  sequential exposures on the  $\text{Al}_2\text{O}_3$  ALD film. The  $\text{BCl}_3$  exposures were at 500 mTorr for 1 s. An Al–CH<sub>3</sub> methyl-terminated  $\text{Al}_2\text{O}_3$  surface was employed to remove the possible reaction of  $\text{BCl}_3$  with Al–OH surface species that would also produce B–O stretching vibrations. These difference spectra are all referenced to the spectrum of the initial  $\text{Al}_2\text{O}_3$  ALD film after the last TMA exposure. Figure 5 shows a loss of absorbance for the Al–O vibrations at 860  $\text{cm}^{-1}$  with an increasing number of  $\text{BCl}_3$  exposures. There is also a gain of absorbance for B–O vibrations at 1370  $\text{cm}^{-1}$  with an increasing number of  $\text{BCl}_3$  exposures.<sup>39</sup> This absorbance loss for Al–O vibrations from  $\text{Al}_2\text{O}_3$  and absorbance gain for B–O vibrations from  $\text{B}_2\text{O}_3$  is clear evidence for the conversion reaction.

The difference spectra in Figure 5 also show evidence for the self-limiting nature of the conversion of  $\text{Al}_2\text{O}_3$  to  $\text{B}_2\text{O}_3$ . The progressive absorbance loss for Al–O vibrations from  $\text{Al}_2\text{O}_3$  and absorbance gain for B–O vibrations from  $\text{B}_2\text{O}_3$  becomes smaller with each successive  $\text{BCl}_3$  exposure. This progressive reduction in the absorbance changes is attributed to the  $\text{B}_2\text{O}_3$  conversion layer on the  $\text{Al}_2\text{O}_3$  surface that acts as a diffusion barrier for  $\text{Al}_2\text{O}_3$  conversion.<sup>48</sup> Additional  $\text{BCl}_3$  exposures must diffuse through the  $\text{B}_2\text{O}_3$  layer to reach the underlying  $\text{Al}_2\text{O}_3$  substrate. In addition, Figure 5 displays a negative absorption feature at 1215  $\text{cm}^{-1}$  that is assigned to the Al–CH<sub>3</sub> deformation mode. The initial  $\text{Al}_2\text{O}_3$  ALD film was methyl-terminated after the TMA exposure. The absorbance from this Al–CH<sub>3</sub> deformation mode is lost during the  $\text{BCl}_3$  conversion reaction.

To visualize the conversion of  $\text{Al}_2\text{O}_3$  to  $\text{B}_2\text{O}_3$ , the integrated absorbance for the Al–O and B–O vibrations versus  $\text{BCl}_3$

exposures is displayed in Figure 6. The integrated absorbance for the Al–O vibrations was determined from 400 to 1050

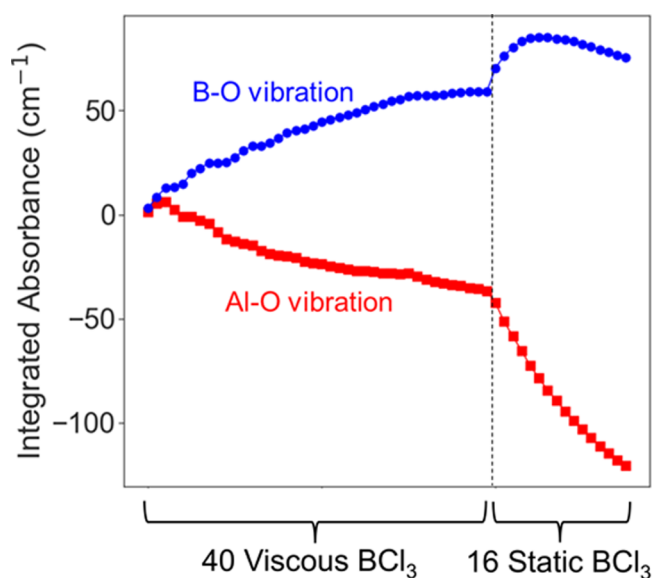


**Figure 6.** Integrated absorbance for B–O vibrations from 1050 to 1800  $\text{cm}^{-1}$  and Al–O vibrations from 400 to 1050  $\text{cm}^{-1}$  from difference spectra during 40 viscous  $\text{BCl}_3$  exposures and 16 static  $\text{BCl}_3$  exposures.

$\text{cm}^{-1}$ . The integrated absorbance for the B–O vibrations was determined from 1050 to 1800  $\text{cm}^{-1}$ . The first 40  $\text{BCl}_3$  exposures were conducted using viscous flow conditions with a  $\text{BCl}_3$  pressure at 500 mTorr for 1 s. The subsequent 16  $\text{BCl}_3$  exposures were static exposures at a pressure at 1 Torr for 5 s. The first 40  $\text{BCl}_3$  exposures display an integrated absorbance decrease for the Al–O vibrations and an integrated absorbance increase for the B–O vibrations. The conversion slows after a larger number of  $\text{BCl}_3$  exposures as the  $\text{B}_2\text{O}_3$  conversion layer progressively acts as a diffusion barrier on  $\text{Al}_2\text{O}_3$ .

After the first 40  $\text{BCl}_3$  exposures, 16 additional  $\text{BCl}_3$  exposures were conducted at a higher pressure of 1 Torr for 5 s. This change in the  $\text{BCl}_3$  exposure conditions increased the conversion of  $\text{Al}_2\text{O}_3$  to  $\text{B}_2\text{O}_3$ . Figure 6 shows that the decrease of the integrated absorbance for the Al–O vibrations is larger with each static  $\text{BCl}_3$  exposure compared with the previous 40  $\text{BCl}_3$  exposures. In contrast, the increase of the integrated absorbance for the B–O vibrations was also larger for the first few static  $\text{BCl}_3$  exposures. However, the integrated absorbance for the B–O vibrations then begins to decrease with progressive static  $\text{BCl}_3$  exposures. This behavior suggests that the static  $\text{BCl}_3$  exposures may be able to spontaneously etch the  $\text{B}_2\text{O}_3$  layer.

**3.2. Mass Spectrometry Studies of  $\text{BCl}_3$  Exposure on  $\text{Al}_2\text{O}_3$  and  $\text{B}_2\text{O}_3$ .** The initial exposures of  $\text{BCl}_3$  on  $\text{Al}_2\text{O}_3$  and  $\text{B}_2\text{O}_3$  were also examined using QMS analysis. Figure 7 shows the mass spectrum during a  $\text{BCl}_3$  exposure on  $\text{Al}_2\text{O}_3$  powder at 300 °C. The  $\text{BCl}_3$  exposures were conducted at 2 Torr above the  $\text{N}_2$  background pressure for 120 s. There was a 300 s purge between successive  $\text{BCl}_3$  exposures. The peaks at  $m/z$  values from 132 to 134 are characteristic of  $\text{AlCl}_3^+$ . The intensity of the different masses in this region are consistent with the natural abundances of the <sup>35</sup>Cl and <sup>37</sup>Cl isotopes.  $\text{AlCl}_3$  is the expected Al volatile product resulting from the conversion of  $\text{Al}_2\text{O}_3$  to  $\text{B}_2\text{O}_3$  by the reaction:  $\text{Al}_2\text{O}_3 + 2\text{BCl}_3(\text{g}) \rightarrow \text{B}_2\text{O}_3 +$

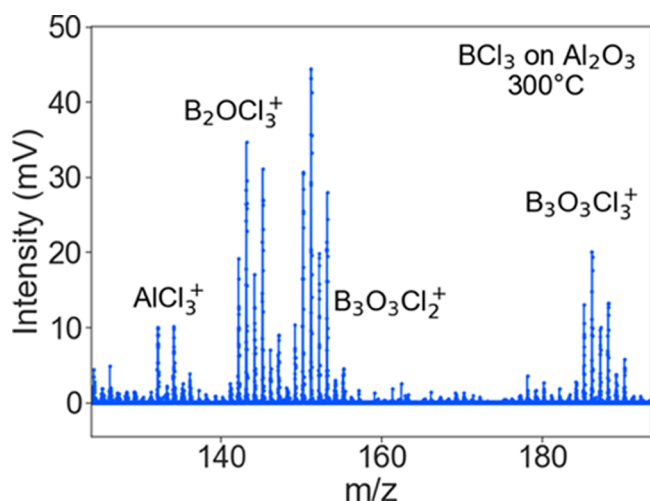


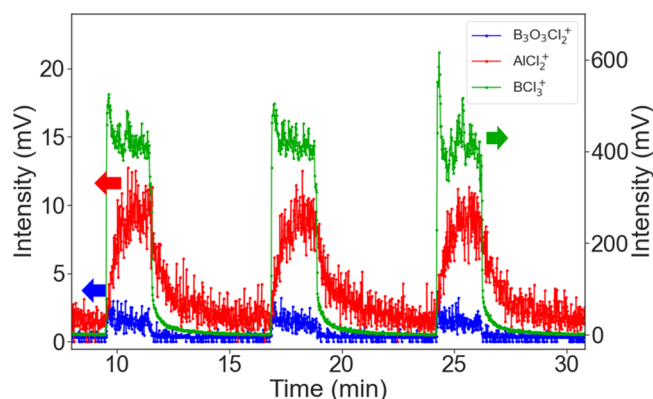
**Figure 7.** Mass spectrum of volatile products from  $\text{BCl}_3$  exposure on  $\text{Al}_2\text{O}_3$  powder at  $300\text{ }^\circ\text{C}$ . Ion signals are attributed to  $\text{AlCl}_3$  and  $\text{B}_3\text{O}_3\text{Cl}_3$  (trichloroboroxin) resulting from conversion of  $\text{Al}_2\text{O}_3$  to  $\text{B}_2\text{O}_3$  and  $\text{BCl}_3$  etching of  $\text{B}_2\text{O}_3$  to produce  $\text{B}_3\text{O}_3\text{Cl}_3$ .

$2\text{AlCl}_3(\text{g})$ . These QMS results corroborate the conversion of  $\text{Al}_2\text{O}_3$  to  $\text{B}_2\text{O}_3$  observed by the FTIR studies in Figure 5.

Figure 7 also reveals a cluster of peaks located at  $m/z$  values from 184 to 190. These peaks are consistent with the ion intensities of  $\text{B}_3\text{O}_3\text{Cl}_3^+$  resulting from the ionization of trichloroboroxin. Trichloroboroxin is a chlorinated boroxine ring molecule. The various peaks represent the masses expected from the natural abundance of the  $^{35}\text{Cl}$  and  $^{37}\text{Cl}$  isotopes and the  $^{10}\text{B}$  and  $^{11}\text{B}$  isotopes. In addition, Figure 7 also has a cluster of masses at  $m/z$  values from 149 to 155 attributed to  $\text{B}_3\text{O}_3\text{Cl}_2^+$ . This ion is a fragment of the  $\text{B}_3\text{O}_3\text{Cl}_3^+$  parent ion. There is also another cluster of masses at  $m/z$  values from 141 to 147 that is assigned to  $\text{B}_2\text{OCl}_3^+$ .

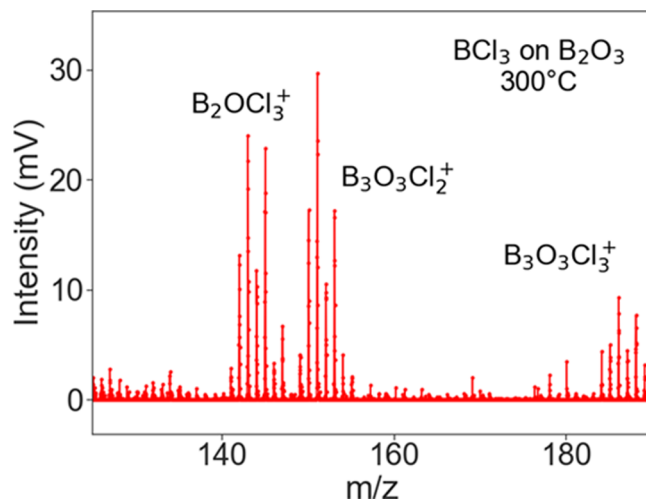
The presence of trichloroboroxin in the mass spectrum during the  $\text{BCl}_3$  exposure on  $\text{Al}_2\text{O}_3$  powder indicates that  $\text{BCl}_3$  can proceed to etch  $\text{B}_2\text{O}_3$  following the conversion of  $\text{Al}_2\text{O}_3$  to  $\text{B}_2\text{O}_3$ . The spontaneous etching of  $\text{B}_2\text{O}_3$  by  $\text{BCl}_3$  can occur by the reaction  $\text{B}_2\text{O}_3 + \text{BCl}_3(\text{g}) \rightarrow \text{B}_3\text{O}_3\text{Cl}_3(\text{g})$ . Thermochemical calculations for this reaction at  $300\text{ }^\circ\text{C}$  yield a small positive standard free energy change of  $\Delta G^\circ = +5.3\text{ kcal/mol}$ .<sup>47</sup> This reaction should not be spontaneous under equilibrium conditions at standard state. However, this reaction may be possible at the nonstandard and nonequilibrium conditions for this surface reaction.

Figure 8 displays the intensities of the  $\text{B}_3\text{O}_3\text{Cl}_2^+$ ,  $\text{AlCl}_2^+$ , and  $\text{BCl}_3^+$  ion signals during three sequential  $\text{BCl}_3$  exposures on the  $\text{Al}_2\text{O}_3$  powder.  $\text{AlCl}_2^+$  is the dominant ion signal in the mass spectrum of  $\text{AlCl}_3$ .<sup>49</sup> The  $\text{AlCl}_2^+$  and  $\text{B}_3\text{O}_3\text{Cl}_2^+$  ion signals are correlated directly with the  $\text{BCl}_3^+$  ion signal. This correlation argues that  $\text{BCl}_3$  converts  $\text{Al}_2\text{O}_3$  to  $\text{B}_2\text{O}_3$  and volatile  $\text{AlCl}_3$ . In addition,  $\text{BCl}_3$  is able to etch  $\text{B}_2\text{O}_3$  and produce volatile  $\text{B}_3\text{O}_3\text{Cl}_3$ . The production of  $\text{AlCl}_3$  and  $\text{B}_3\text{O}_3\text{Cl}_3$  occurs consistently with each  $\text{BCl}_3$  exposure in Figure 8. There is no sign of any decrease of the  $\text{AlCl}_2^+$  and  $\text{B}_3\text{O}_3\text{Cl}_2^+$  ion signals with successive  $\text{BCl}_3$  exposures. This behavior argues that the  $\text{BCl}_3$  etching of  $\text{B}_2\text{O}_3$  is spontaneous. In addition, the removal of  $\text{B}_2\text{O}_3$  by  $\text{BCl}_3$  allows  $\text{BCl}_3$  to continue to convert  $\text{Al}_2\text{O}_3$  to more  $\text{B}_2\text{O}_3$ . These results indicate that  $\text{BCl}_3$  should be able to etch  $\text{Al}_2\text{O}_3$  continuously by this conversion and spontaneous etching mechanism.



**Figure 8.** Time-dependent ion signals for  $\text{B}_3\text{O}_3\text{Cl}_2^+$ ,  $\text{AlCl}_2^+$ , and  $\text{BCl}_3^+$  for three successive  $\text{BCl}_3$  exposures on  $\text{Al}_2\text{O}_3$  powder at  $300\text{ }^\circ\text{C}$ .  $\text{B}_3\text{O}_3\text{Cl}_2^+$ ,  $\text{AlCl}_2^+$ , and  $\text{BCl}_3^+$  ion signals are monitored at  $m/z$  values of 186, 97, and 116, respectively.

To confirm that  $\text{BCl}_3$  can spontaneously etch  $\text{B}_2\text{O}_3$ , additional QMS experiments were performed using  $\text{BCl}_3$  exposures on  $\text{B}_2\text{O}_3$  powder. Figure 9 displays QMS results



**Figure 9.** Mass spectrum of volatile products from  $\text{BCl}_3$  exposure on  $\text{B}_2\text{O}_3$  powder at  $300\text{ }^\circ\text{C}$ . Ion signals are attributed to  $\text{B}_3\text{O}_3\text{Cl}_3$  (trichloroboroxin) resulting from  $\text{BCl}_3$  etching of  $\text{B}_2\text{O}_3$ .

for  $\text{BCl}_3$  exposures on  $\text{B}_2\text{O}_3$  powder at  $300\text{ }^\circ\text{C}$ . The results in Figure 9 are nearly identical to the results for  $\text{BCl}_3$  exposure on  $\text{Al}_2\text{O}_3$  powder shown in Figure 7. The difference is the absence of  $\text{AlCl}_3^+$  ion signals in Figure 9. There is no conversion of  $\text{Al}_2\text{O}_3$  to  $\text{B}_2\text{O}_3$  occurring when  $\text{BCl}_3$  exposures are incident on  $\text{B}_2\text{O}_3$  powder. Consequently, there are no  $\text{AlCl}_3$  products produced that could yield  $\text{AlCl}_3^+$  ion signals. Similar to the results in Figure 7, the results in Figure 9 are consistent with the spontaneous etching reaction:  $\text{B}_2\text{O}_3 + \text{BCl}_3(\text{g}) \rightarrow \text{B}_3\text{O}_3\text{Cl}_3(\text{g})$ .

Figure 10 shows the  $\text{B}_3\text{O}_3\text{Cl}_2^+$  and  $\text{BCl}_3^+$  ion signals during sequential  $\text{BCl}_3$  exposures on the  $\text{B}_2\text{O}_3$  powder. The  $\text{B}_3\text{O}_3\text{Cl}_2^+$  ion signals are coincident with the  $\text{BCl}_3^+$  ion signal. This coincidence demonstrates that  $\text{BCl}_3$  can etch  $\text{B}_2\text{O}_3$  and produce trichloroboroxin as the etch product. There is no decrease of  $\text{B}_3\text{O}_3\text{Cl}_2^+$  ion signals with an increasing number of  $\text{BCl}_3$  exposures. This behavior argues that  $\text{BCl}_3$  can spontaneously etch  $\text{B}_2\text{O}_3$  and produce  $\text{B}_3\text{O}_3\text{Cl}_3$  with nothing

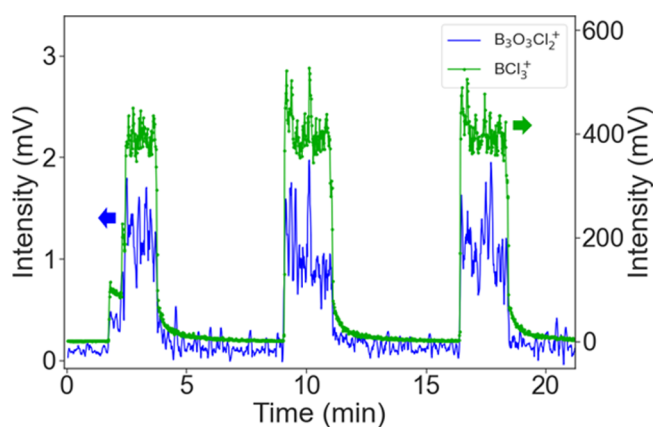


**Figure 10.** Time-dependent ion signals for  $B_3O_3Cl_2^+$  and  $BCl_3^+$  for three successive  $BCl_3$  exposures on  $B_2O_3$  powder at  $300\text{ }^\circ\text{C}$ .  $B_3O_3Cl_2^+$  and  $BCl_3^+$  ion signals are monitored at  $m/z$  values of 186 and 116, respectively.

building up on the surface that could decrease the spontaneous etching.

### 3.3. FTIR Studies of Sequential HF and $BCl_3$ Exposures after Initial $BCl_3$ Exposure.

Figure 11 shows

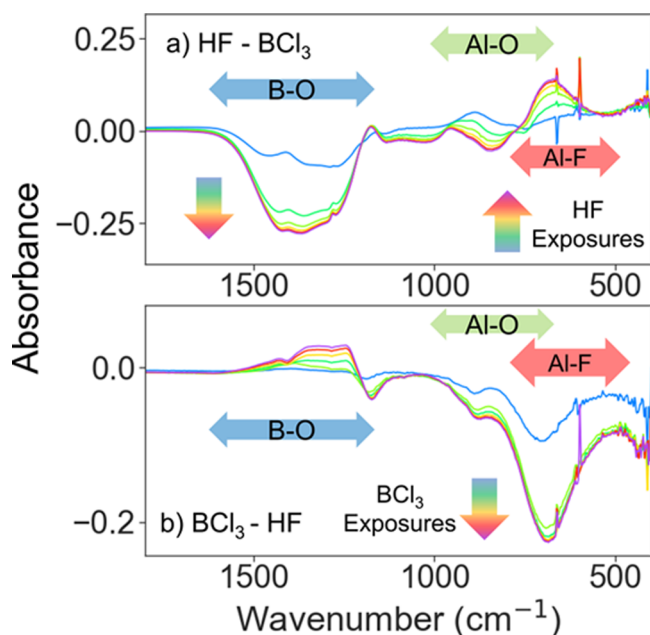


**Figure 11.** (a) FTIR difference spectra during 20 HF exposures at  $300\text{ }^\circ\text{C}$  immediately following the  $BCl_3$  exposures on  $Al_2O_3$  shown in Figure 5. (b) FTIR difference spectra during 20  $BCl_3$  exposures at  $300\text{ }^\circ\text{C}$  immediately following the HF exposures shown in (a).

the difference spectra for the subsequent HF and  $BCl_3$  exposures after the  $BCl_3$  exposures on the  $Al_2O_3$  ALD films that were presented earlier in Figure 5. The results in Figure 5 for the  $BCl_3$  exposures displayed an absorbance loss at  $860\text{ cm}^{-1}$  corresponding to the Al–O vibrations and an absorbance gain at  $1370\text{ cm}^{-1}$  corresponding to the B–O vibrations. These results were consistent with the conversion of  $Al_2O_3$  to  $B_2O_3$ . On the subsequent HF exposures at  $200\text{ mTorr}$  for 1 s, the difference spectra in Figure 11a display a large decrease in absorbance from  $1100\text{--}1600\text{ cm}^{-1}$ . This absorbance loss is consistent with the removal of absorbance from the B–O

vibrations in  $B_2O_3$  formed by the previous  $BCl_3$  exposure on  $Al_2O_3$ .

These results indicate that HF can spontaneously etch  $B_2O_3$  by the reaction  $B_2O_3 + 6HF(g) \rightarrow 2BF_3(g) + 3H_2O(g)$ , as illustrated in Figure 2. This spontaneous etching of  $B_2O_3$  by HF has been investigated by earlier studies.<sup>10,39</sup> Thermochemical calculations for this reaction at  $300\text{ }^\circ\text{C}$  yield a negative standard free energy change of  $\Delta G^0 = -16.4\text{ kcal/mol}$ .<sup>47</sup> This negative standard free energy change predicts a spontaneous reaction under equilibrium conditions at the standard state. In addition, this negative standard free energy change also suggests that the reaction would likely be spontaneous under the nonstandard and nonequilibrium conditions for this surface reaction.

In addition to removing  $B_2O_3$ , the HF exposure is also able to fluorinate  $Al_2O_3$ . Figure 11a shows an increase in absorbance at  $680\text{ cm}^{-1}$ . This absorbance is attributed to the Al–F stretching vibrations in  $AlF_3$ . This absorbance feature for the Al–F stretching vibration has been observed earlier in studies of  $Al_2O_3$  fluorination.<sup>21</sup> In addition, this Al–F stretching vibration has been monitored during  $Al_2O_3$  ALE using fluorination and ligand-exchange reactions.<sup>7,21</sup>

The difference spectra for the next 20  $BCl_3$  exposures at  $500\text{ mTorr}$  for 1 s after the previous HF exposures are shown in Figure 11b. These difference spectra are not identical to difference spectra for the  $BCl_3$  exposures on the initial  $Al_2O_3$  ALD film shown in Figure 5. The absorbance gain for the B–O vibrations at  $1370\text{ cm}^{-1}$  in Figure 11b is much smaller than the absorbance gain for the B–O vibrations in Figure 5 for the initial  $BCl_3$  exposures. There is also a pronounced absorbance loss at  $690\text{ cm}^{-1}$  with the  $BCl_3$  exposures. This absorbance loss is red-shifted relative to the absorbance loss at  $860\text{ cm}^{-1}$  in Figure 5.

This absorbance loss at  $690\text{ cm}^{-1}$  is attributed to the reduction of Al–F stretching vibrations resulting from the ligand-exchange reaction of  $BCl_3$  with  $AlF_3$ . The ligand-exchange reaction volatilizes the  $AlF_3$  layer and can be expressed as  $AlF_3 + 3BCl_3(g) \rightarrow AlCl_3(g) + 3BFCl_2(g)$  if each  $BCl_3$  reactant undergoes only one ligand-exchange reaction. The reaction could also be expressed as  $AlF_3 + BCl_3(g) \rightarrow AlCl_3(g) + BF_3(g)$  if each  $BCl_3$  reactant undergoes three ligand-exchange reactions. In addition, the absorbance loss is also caused by more conversion of  $Al_2O_3$  to  $B_2O_3$  by the  $BCl_3$  exposures according to  $Al_2O_3 + 2BCl_3(g) \rightarrow B_2O_3 + 2AlCl_3(g)$ . This conversion reaction leads to additional reduction of absorbance for the Al–O vibrations from  $Al_2O_3$ .

The difference spectra evolved during the subsequent HF and  $BCl_3$  exposures during  $Al_2O_3$  ALE. Figure 12 shows the difference spectra after HF and  $BCl_3$  exposures in the steady state regime of  $Al_2O_3$  ALE. The difference spectra are referenced to the spectra after the previous exposure. In Figure 12a for the difference spectrum corresponding to HF– $BCl_3$ , there are absorbance increases at  $690$  and  $900\text{ cm}^{-1}$  resulting from the HF exposure. These absorbance increases are consistent with formation of more  $AlF_3$  and Al–F stretching vibrations by the fluorination of  $Al_2O_3$  to  $AlF_3$  as shown in Figure 1.<sup>7,21</sup> There is also a slight reduction in absorbance from  $1100$  to  $1600\text{ cm}^{-1}$  in the region corresponding to the B–O vibrations in  $B_2O_3$ . The HF exposure is able to remove the  $B_2O_3$  formed by the previous  $BCl_3$  exposure as displayed in Figure 2.

In Figure 12b for the difference spectrum corresponding to  $BCl_3$ –HF, there are absorbance decreases at  $690$  and  $900\text{ cm}^{-1}$

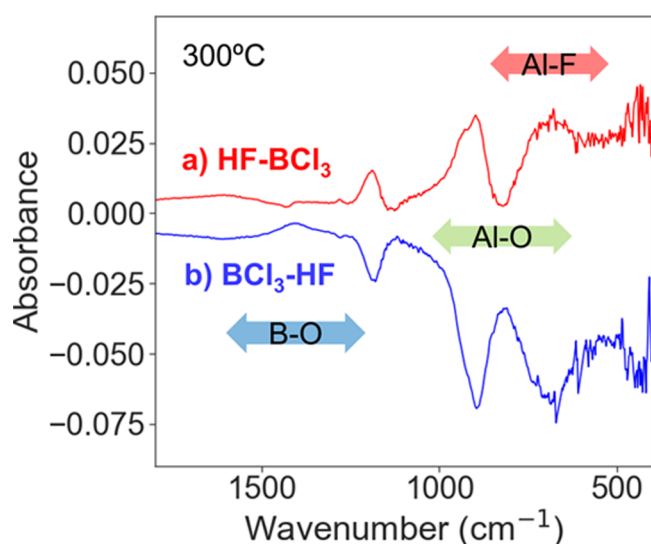


**Figure 12.** Difference spectra during steady state thermal  $\text{Al}_2\text{O}_3$  ALE at 300 °C. (a) FTIR difference spectra after HF exposure referenced to previous  $\text{BCl}_3$  exposure and (b) FTIR difference spectra after  $\text{BCl}_3$  exposure referenced to previous HF exposure.

resulting from the  $\text{BCl}_3$  exposure. These are the same Al–F vibrational features that were produced during the HF exposure. The  $\text{BCl}_3$  exposure is able to remove these Al–F vibrational features by ligand-exchange reactions as illustrated in Figure 1. There is also a slight increase in absorbance from 1100 to 1600  $\text{cm}^{-1}$  in the region corresponding to the B–O vibrations in  $\text{B}_2\text{O}_3$ . The  $\text{BCl}_3$  exposure is able to convert more  $\text{Al}_2\text{O}_3$  to  $\text{B}_2\text{O}_3$  after removing the  $\text{AlF}_3$  layer on the  $\text{Al}_2\text{O}_3$  surface.

**3.4. Spectroscopic Ellipsometry Measurements of Etch Rates and Mass Spectrometry Studies in Steady State.** The sequential exposures of HF and  $\text{BCl}_3$  lead to thermal  $\text{Al}_2\text{O}_3$  ALE. The etch rates of  $\text{Al}_2\text{O}_3$  were obtained using spectroscopic ellipsometry measurements. Figure 13 shows the thickness measurements during  $\text{Al}_2\text{O}_3$  ALE using HF and  $\text{BCl}_3$  at a variety of temperatures. The HF exposure was 100 mTorr for 1 s, and the  $\text{BCl}_3$  exposure was at 500

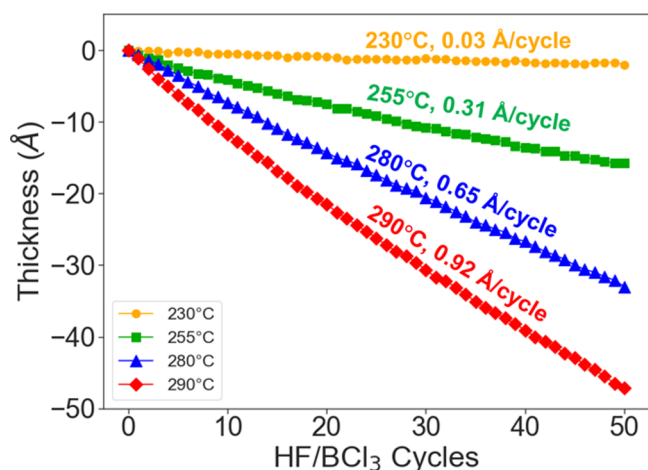


**Figure 13.** Spectroscopic ellipsometry measurements of  $\text{Al}_2\text{O}_3$  thickness loss during  $\text{Al}_2\text{O}_3$  ALE using HF and  $\text{BCl}_3$  as reactants at variety of temperatures. Etch rates were 0.03, 0.31, 0.65, and 0.92 Å/cycle at 230, 255, 280, and 290 °C, respectively.

mTorr for 1 s. There was a purge time of 60 s between each reactant exposure. The etch rates were 0.03, 0.31, 0.65, and 0.92 Å/cycle at temperatures of 230, 255, 280, and 290 °C, respectively. The uncertainties of these etch rates were  $\pm 0.004$ , 0.005, 0.006, and 0.006 Å/cycle, respectively. These uncertainties were determined by the error in the linear fits.

Progressively larger etch rates at higher temperatures have been observed previously for thermal ALE systems.<sup>7,20,27</sup> The larger etch rates at higher temperatures could be attributed to either greater fluorination or more complete ligand-exchange reactions at higher temperatures.<sup>7,27</sup> In addition, the temperature-dependent etch rates could result from more efficient conversion of  $\text{Al}_2\text{O}_3$  to  $\text{B}_2\text{O}_3$  at higher temperatures. Understanding the temperature dependence resulting from the fluorination and ligand-exchange mechanism or the conversion and spontaneous etching mechanism would require detailed QMS analysis of the reaction products at different temperatures.

QMS analysis was performed during the HF and  $\text{BCl}_3$  exposures in the steady state regime during  $\text{Al}_2\text{O}_3$  ALE at 270 °C. The mass spectrum during the HF exposure for the 5th  $\text{Al}_2\text{O}_3$  ALE cycle is shown in Figure 14a. The HF exposure

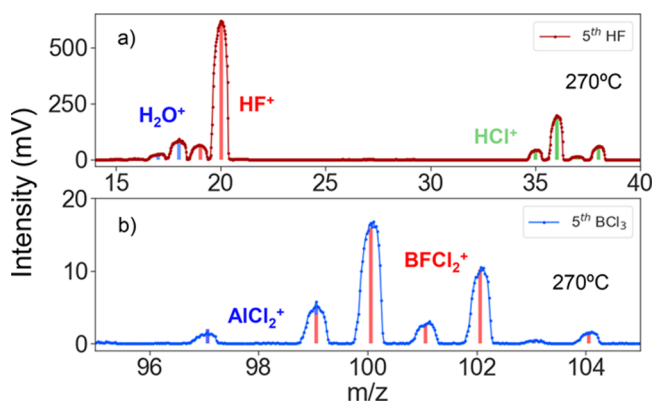


**Figure 14.** Mass spectrum during the fifth thermal  $\text{Al}_2\text{O}_3$  ALE cycle on  $\text{Al}_2\text{O}_3$  powder. (a) Mass spectrum during the fifth HF exposure observing  $\text{H}_2\text{O}^+$ ,  $\text{HF}^+$ , and  $\text{HCl}^+$  ion signals. (b) Mass spectrum during the fifth  $\text{BCl}_3$  exposure observing  $\text{AlCl}_2^+$  and  $\text{BCl}_2^+$  ion signals.

was 2 Torr over the  $\text{N}_2$  background pressure for 120 s. The QMS analysis detects a number of species including  $\text{H}_2\text{O}$ , HF, and HCl. HF is expected because HF is the reactant.  $\text{H}_2\text{O}$  is also anticipated because  $\text{H}_2\text{O}$  is a product of the fluorination reaction:  $\text{Al}_2\text{O}_3 + \text{HF}(\text{g}) \rightarrow 2\text{AlF}_3 + 3\text{H}_2\text{O}(\text{g})$  as shown in Figure 1. Thermochemical calculations for this reaction at 270 °C yield a large negative standard free energy change of  $\Delta G^0 = -51.9$  kcal/mol.<sup>47</sup> The HCl is attributed to residual chlorine left on the  $\text{Al}_2\text{O}_3$  surface after the  $\text{BCl}_3$  exposure. HCl could be formed by HF exchange with surface chlorine by the reaction:  $\text{Al-Cl} + \text{HF}(\text{g}) \rightarrow \text{Al-F} + \text{HCl}(\text{g})$ .

There were also no boron-containing species observed by the QMS analysis during the HF exposures. Earlier QMS studies observed  $\text{BF}_3$ ,  $\text{BF}_2\text{OH}$ , and various boroxine ring molecules, such as  $\text{B}_3\text{O}_3\text{F}_3$  and  $\text{B}_3\text{O}_3\text{F}_2(\text{OH})$ , during HF exposures on  $\text{B}_2\text{O}_3$  powder.<sup>39</sup> These boron-containing species may be below the detection limit for the QMS analysis. In addition, the lack of boron-containing species suggests that the primary mechanism for  $\text{Al}_2\text{O}_3$  ALE using HF and  $\text{BCl}_3$  in steady state is by HF fluorination of  $\text{Al}_2\text{O}_3$  to  $\text{AlF}_3$  and then

ligand-exchange reactions between  $\text{BCl}_3$  and  $\text{AlF}_3$  to form volatile  $\text{BF}_3$  and  $\text{AlCl}_3$  products.

To explore the volatile products during the  $\text{BCl}_3$  reaction, Figure 14b shows the QMS analysis for  $m/z$  values from 95 to 107 during the  $\text{BCl}_3$  exposure for the 5th  $\text{Al}_2\text{O}_3$  ALE cycle on the  $\text{Al}_2\text{O}_3$  powder at 270 °C. The  $\text{BCl}_3$  exposure was 2 Torr over the  $\text{N}_2$  background pressure for 120 s. The QMS measurements observe ion intensities for  $\text{AlCl}_2^+$  and  $\text{BFCl}_2^+$ .  $\text{AlCl}_2^+$  at an  $m/z$  value of 97 is the most intense cracking fragment of the  $\text{AlCl}_3$  parent.<sup>49</sup>  $\text{AlCl}_3$  is expected from the ligand-exchange reaction  $\text{AlF}_3 + 3\text{BCl}_3(\text{g}) \rightarrow \text{AlCl}_3(\text{g}) + 3\text{BFCl}_2(\text{g})$ , as displayed in Figure 1.  $\text{AlCl}_3$  is also possible from the conversion reaction  $\text{Al}_2\text{O}_3 + 2\text{BCl}_3(\text{g}) \rightarrow \text{B}_2\text{O}_3 + 2\text{AlCl}_3(\text{g})$ , as shown in Figure 2.

An ion signal is also detected for  $\text{BFCl}_2^+$  with the largest signal at an  $m/z$  value of 100 in Figure 14b.  $\text{BFCl}_2$  would be produced by a single ligand exchange between  $\text{BCl}_3$  and the  $\text{AlF}_3$  surface. Small peaks that were consistent with  $\text{BF}_2\text{Cl}$  were also observed in the QMS spectrum (not shown). There was no evidence for  $\text{BF}_3$  that would indicate three ligand-exchange reactions between  $\text{BCl}_3$  and the  $\text{AlF}_3$  surface. In addition, there were small amounts of  $\text{B}_3\text{O}_3\text{Cl}_3$  present in the QMS spectrum with a low intensity of  $\sim 0.5$  mV during  $\text{BCl}_3$  exposures. The removal of  $\text{B}_2\text{O}_3$  by  $\text{BCl}_3$  to yield trichloroboroxin may have reduced the quantity of boron-containing species that could have otherwise been observed during the spontaneous etching of  $\text{B}_2\text{O}_3$  by the HF exposures.

#### 4. CONCLUSIONS

$\text{BCl}_3$  is a new reactant for thermal  $\text{Al}_2\text{O}_3$  ALE.  $\text{BCl}_3$  has the potential to enable thermal ALE through either ligand-exchange or conversion reaction mechanisms. FTIR spectroscopy and QMS analysis revealed that initial  $\text{BCl}_3$  exposures on  $\text{Al}_2\text{O}_3$  converted the  $\text{Al}_2\text{O}_3$  surface to a  $\text{B}_2\text{O}_3$  layer. The FTIR studies observed the absorbance loss of Al–O vibrations from  $\text{Al}_2\text{O}_3$  and the absorbance gain of B–O vibrations from  $\text{B}_2\text{O}_3$  with  $\text{BCl}_3$  exposures. The QMS investigations also observed ion intensities for  $\text{AlCl}_3^+$  from  $\text{AlCl}_3$  during the conversion of  $\text{Al}_2\text{O}_3$  to  $\text{B}_2\text{O}_3$ .

Larger  $\text{BCl}_3$  exposures on the converted  $\text{B}_2\text{O}_3$  layer on  $\text{Al}_2\text{O}_3$  were also observed to etch the  $\text{B}_2\text{O}_3$  layer. The FTIR studies observed the absorbance loss of B–O vibrations from  $\text{B}_2\text{O}_3$  for larger  $\text{BCl}_3$  exposures. The QMS investigations also monitored ion intensities for  $\text{B}_3\text{O}_3\text{Cl}_3^+$  from trichloroboroxin during  $\text{BCl}_3$  exposures.  $\text{BCl}_3$  plays the unique role of first producing  $\text{B}_2\text{O}_3$  from the conversion of  $\text{Al}_2\text{O}_3$ . Subsequently, the  $\text{BCl}_3$  can etch the  $\text{B}_2\text{O}_3$  conversion product. Additional QMS studies confirmed that  $\text{BCl}_3$  could etch initial  $\text{B}_2\text{O}_3$  substrates through the formation of  $\text{B}_3\text{O}_3\text{Cl}_3$  boroxine ring products.

During the HF and  $\text{BCl}_3$  exposures for thermal  $\text{Al}_2\text{O}_3$  ALE in steady state, the FTIR difference spectra indicated that  $\text{Al}_2\text{O}_3$  ALE proceeded mostly by a reaction pathway where HF fluorinates the  $\text{Al}_2\text{O}_3$  to  $\text{AlF}_3$  and then  $\text{BCl}_3$  removes the  $\text{AlF}_3$  layer by a ligand-exchange reaction. There was also evidence for some conversion of  $\text{Al}_2\text{O}_3$  to a  $\text{B}_2\text{O}_3$  layer during the  $\text{BCl}_3$  exposures and then removal of the  $\text{B}_2\text{O}_3$  layer by the HF exposures. In support of the ligand-exchange mechanism, the QMS measurements observed ion intensities for  $\text{BFCl}_2^+$  and  $\text{AlCl}_2^+$  during the  $\text{BCl}_3$  exposures in steady state. Small ion intensities for  $\text{B}_3\text{O}_3\text{Cl}_3^+$  were also detected that were consistent with some conversion of  $\text{Al}_2\text{O}_3$  to  $\text{B}_2\text{O}_3$  and the subsequent etching of  $\text{B}_2\text{O}_3$  by  $\text{BCl}_3$ . The QMS measurements also

monitored ion intensities for  $\text{H}_2\text{O}^+$  and  $\text{HCl}^+$  during the HF exposures.

Spectroscopic ellipsometry (SE) measurements also measured the etch rates during thermal  $\text{Al}_2\text{O}_3$  ALE. The etch rates increased progressively at higher temperatures. The etch rates were 0.03 Å/cycle at 230 °C, 0.31 Å/cycle at 255 °C, 0.65 Å/cycle at 280 °C, and 0.92 Å/cycle at 290 °C. Thermal  $\text{Al}_2\text{O}_3$  ALE using sequential HF and  $\text{BCl}_3$  exposures occurs by a combination of ligand-exchange and conversion mechanisms and provides another pathway for thermal  $\text{Al}_2\text{O}_3$  ALE. This new pathway should be useful to define area selective etching procedures for  $\text{Al}_2\text{O}_3$  and other materials.

#### ■ AUTHOR INFORMATION

##### Corresponding Author

Steven M. George – Department of Chemistry, University of Colorado, Boulder, Colorado 80309, United States;

orcid.org/0000-0003-0253-9184;

Email: Steven.George@Colorado.edu

##### Authors

Austin M. Cano – Department of Chemistry, University of Colorado, Boulder, Colorado 80309, United States

Jonathan L. Partridge – Department of Chemistry, University of Colorado, Boulder, Colorado 80309, United States;

orcid.org/0000-0002-0071-9854

Complete contact information is available at:

<https://pubs.acs.org/10.1021/acs.chemmater.2c01120>

##### Notes

The authors declare no competing financial interest.

#### ■ ACKNOWLEDGMENTS

The FTIR and SE studies were funded by Intel through a member specific research grant from the Semiconductor Research Corporation (SRC). Funding for the QMS reactor and the QMS investigations was provided by Lam Research.

#### ■ REFERENCES

- (1) George, S. M. Mechanisms of Thermal Atomic Layer Etching. *Acc. Chem. Res.* **2020**, *53*, 1151–1160.
- (2) Kanarik, K. J.; Lill, T.; Hudson, E. A.; Sriraman, S.; Tan, S.; Marks, J.; Vahedi, V.; Gottscho, R. A. Overview of Atomic Layer Etching in the Semiconductor Industry. *J. Vac. Sci. Technol., A* **2015**, *33*, No. 020802.
- (3) Fischer, A.; Routzahn, A.; George, S. M.; Lill, T. Thermal Atomic Layer Etching: A Review. *J. Vac. Sci. Technol., A* **2021**, *39*, No. 030801.
- (4) George, S. M.; Lee, Y. Prospects for Thermal Atomic Layer Etching Using Sequential, Self-Limiting Fluorination and Ligand-Exchange Reactions. *ACS Nano* **2016**, *10*, 4889–4894.
- (5) Gertsch, J. C.; Cano, A. M.; Bright, V. M.; George, S. M.  $\text{SF}_4$  as the Fluorination Reactant for  $\text{Al}_2\text{O}_3$  and  $\text{VO}_2$  Thermal Atomic Layer Etching. *Chem. Mater.* **2019**, *31*, 3624–3635.
- (6) Johnson, N. R.; Hite, J. K.; Mastro, M. A.; Eddy, C. R.; George, S. M. Thermal Atomic Layer Etching of Crystalline GaN Using Sequential Exposures of  $\text{XeF}_2$  and  $\text{BCl}_3$ . *Appl. Phys. Lett.* **2019**, *114*, 243103.
- (7) Lee, Y.; DuMont, J. W.; George, S. M. Trimethylaluminum as the Metal Precursor for the Atomic Layer Etching of  $\text{Al}_2\text{O}_3$  Using Sequential Self-Limiting Thermal Reactions. *Chem. Mater.* **2016**, *28*, 2994–3003.
- (8) Lii-Rosales, A.; Cavanagh, A. S.; Fischer, A.; Lill, T.; George, S. M. Spontaneous Etching of Metal Fluorides Using Ligand-Exchange

Reactions: Landscape Revealed by Mass Spectrometry. *Chem. Mater.* **2021**, *33*, 7719–7730.

(9) DuMont, J. W.; Marquardt, A. E.; Cano, A. M.; George, S. M. Thermal Atomic Layer Etching of SiO<sub>2</sub> by a "Conversion-Etch" Mechanism Using Sequential Reactions of Trimethylaluminum and Hydrogen Fluoride. *ACS Appl. Mater. Interfaces* **2017**, *9*, 10296–10307.

(10) Johnson, N. R.; George, S. M. WO<sub>3</sub> and W Thermal Atomic Layer Etching Using "Conversion-Fluorination" and "Oxidation-Conversion-Fluorination" Mechanisms. *ACS Appl. Mater. Interfaces* **2017**, *9*, 34435–34447.

(11) Myers, T. J.; Cano, A. M.; Lancaster, D. K.; Clancey, J. W.; George, S. M. Conversion Reactions in Atomic Layer Processing with Emphasis on ZnO Conversion to Al<sub>2</sub>O<sub>3</sub> by Trimethylaluminum. *J. Vac. Sci. Technol., A* **2021**, *39*, No. 021001.

(12) Zywojtko, D. R.; George, S. M. Thermal Atomic Layer Etching of ZnO by a "Conversion-Etch" Mechanism Using Sequential Exposures of Hydrogen Fluoride and Trimethylaluminum. *Chem. Mater.* **2017**, *29*, 1183–1191.

(13) Abdulagatov, A. I.; George, S. M. Thermal Atomic Layer Etching of Silicon Using O<sub>2</sub>, HF, and Al(CH<sub>3</sub>)<sub>3</sub> as the Reactants. *Chem. Mater.* **2018**, *30*, 8465–8475.

(14) Abdulagatov, A. I.; George, S. M. Thermal Atomic Layer Etching of Silicon Nitride Using an Oxidation and "Conversion Etch" Mechanism. *J. Vac. Sci. Technol., A* **2020**, *38*, No. 022607.

(15) Murdzek, J. A.; Lii-Rosales, A.; George, S. M. Thermal Atomic Layer Etching of Nickel Using Sequential Chlorination and Ligand-Addition Reactions. *Chem. Mater.* **2021**, *33*, 9174–9183.

(16) Mohimi, E.; Chu, X. Q. L.; Trinh, B. B.; Babar, S.; Girolami, G. S.; Abelson, J. R. Thermal Atomic Layer Etching of Copper by Sequential Steps Involving Oxidation and Exposure to Hexafluoroacetylacetonone. *ECS J. Solid State Sci. Technol.* **2018**, *7*, P491–P495.

(17) Konh, M.; He, C.; Lin, X.; Guo, X. Y.; Pallem, V.; Opila, R. L.; Teplyakov, A. V.; Wang, Z. J.; Yuan, B. Molecular Mechanisms of Atomic Layer Etching of Cobalt with Sequential Exposure to Molecular Chlorine and Diketones. *J. Vac. Sci. Technol., A* **2019**, *37*, No. 021004.

(18) Lin, X.; Chen, M. X.; Janotti, A.; Opila, R. In situ XPS Study on Atomic Layer Etching of Fe Thin Film Using Cl<sub>2</sub> and Acetylacetonone. *J. Vac. Sci. Technol., A* **2018**, *36*, No. 051401.

(19) Lee, Y.; George, S. M. Atomic Layer Etching of Al<sub>2</sub>O<sub>3</sub> Using Sequential, Self-Limiting Thermal Reactions with Sn(acac)<sub>2</sub> and Hydrogen Fluoride. *ACS Nano* **2015**, *9*, 2061–2070.

(20) Lee, Y.; DuMont, J. W.; George, S. M. Mechanism of Thermal Al<sub>2</sub>O<sub>3</sub> Atomic Layer Etching Using Sequential Reactions with Sn(acac)<sub>2</sub> and HF. *Chem. Mater.* **2015**, *27*, 3648–3657.

(21) Cano, A. M.; Marquardt, A. E.; DuMont, J. W.; George, S. M. Effect of HF Pressure on Thermal Al<sub>2</sub>O<sub>3</sub> Atomic Layer Etch Rates and Al<sub>2</sub>O<sub>3</sub> Fluorination. *J. Phys. Chem. C* **2019**, *123*, 10346–10355.

(22) DuMont, J. W.; George, S. M. Competition Between Al<sub>2</sub>O<sub>3</sub> Atomic Layer Etching and AlF<sub>3</sub> Atomic Layer Deposition Using Sequential Exposures of Trimethylaluminum and Hydrogen Fluoride. *J. Chem. Phys.* **2017**, *146*, No. 052819.

(23) Fischer, A.; Routzahn, A.; Lee, Y.; Lill, T.; George, S. M. Thermal Etching of AlF<sub>3</sub> and Thermal Atomic Layer Etching of Al<sub>2</sub>O<sub>3</sub>. *J. Vac. Sci. Technol., A* **2020**, *38*, No. 022603.

(24) Gertsch, J. C.; Sortino, E.; Bright, V. M.; George, S. M. Deposit and Etchback Approach for Ultrathin Al<sub>2</sub>O<sub>3</sub> Films with Low Pinhole Density Using Atomic Layer Deposition and Atomic Layer Etching. *J. Vac. Sci. Technol., A* **2021**, *39*, No. 062602.

(25) Hennessy, J.; Jewell, A. D.; Jones, J. P.; Crouch, G. M.; Nikzad, S. Aluminum Precursor Interactions with Alkali Compounds in Thermal Atomic Layer Etching and Deposition Processes. *ACS Appl. Mater. Interfaces* **2021**, *13*, 4723–4730.

(26) Hennessy, J.; Moore, C. S.; Balasubramanian, K.; Jewell, A. D.; France, K.; Nikzad, S. Enhanced Atomic Layer Etching of Native Aluminum Oxide for Ultraviolet Optical Applications. *J. Vac. Sci. Technol., A* **2017**, *35*, No. 041512.

(27) Lee, Y.; George, S. M. Thermal Atomic Layer Etching of Al<sub>2</sub>O<sub>3</sub>, HfO<sub>2</sub>, and ZrO<sub>2</sub> Using Sequential Hydrogen Fluoride and Dimethylaluminum Chloride Exposures. *J. Phys. Chem. C* **2019**, *123*, 18455–18466.

(28) Murdzek, J. A.; Rajashekhar, A.; Makala, R. S.; George, S. M. Thermal Atomic Layer Etching of Amorphous and Crystalline Al<sub>2</sub>O<sub>3</sub> films. *J. Vac. Sci. Technol., A* **2021**, *39*, No. 042602.

(29) Rahman, R.; Mattson, E. C.; Klesko, J. P.; Dangerfield, A.; Rivillon-Amy, S.; Smith, D. C.; Hausmann, D.; Chabal, Y. J. Thermal Atomic Layer Etching of Silica and Alumina Thin Films Using Trimethylaluminum with Hydrogen Fluoride or Fluoroform. *ACS Appl. Mater. Interfaces* **2018**, *10*, 31784–31794.

(30) Zywojtko, D. R.; Faguet, J.; George, S. M. Rapid Atomic Layer Etching of Al<sub>2</sub>O<sub>3</sub> Using Sequential Exposures of Hydrogen Fluoride and Trimethylaluminum with No Purging. *J. Vac. Sci. Technol., A* **2018**, *36*, No. 061508.

(31) Zywojtko, D. R.; Zandi, O.; Faguet, J.; Abel, P. R.; George, S. M. ZrO<sub>2</sub> Monolayer as a Removable Etch Stop Layer for Thermal Al<sub>2</sub>O<sub>3</sub> Atomic Layer Etching Using Hydrogen Fluoride and Trimethylaluminum. *Chem. Mater.* **2020**, *32*, 10055–10065.

(32) Clancey, J. W.; Cavanagh, A. S.; Smith, J. E. T.; Sharma, S.; George, S. M. Volatile Etch Species Produced during Thermal Al<sub>2</sub>O<sub>3</sub> Atomic Layer Etching. *J. Phys. Chem. C* **2020**, *124*, 287–299.

(33) Sharma, V.; Elliott, S. D.; Blomberg, T.; Haukka, S.; Givens, M. E.; Tuominen, M.; Ritala, M. Thermal Atomic Layer Etching of Aluminum Oxide (Al<sub>2</sub>O<sub>3</sub>) Using Sequential Exposures of Niobium Pentafluoride (NbF<sub>5</sub>) and Carbon Tetrachloride (CCl<sub>4</sub>): A Combined Experimental and Density Functional Theory Study of the Etch Mechanism. *Chem. Mater.* **2021**, *33*, 2883–2893.

(34) Chittock, N. J.; Vos, M. F. J.; Faraz, T.; Kessels, W. M. M.; Knoops, H. C. M.; Mackus, A. J. M. Isotropic Plasma Atomic Layer Etching of Al<sub>2</sub>O<sub>3</sub> Using a Fluorine Containing Plasma and Al(CH<sub>3</sub>)<sub>3</sub>. *Appl. Phys. Lett.* **2020**, *117*, 162107.

(35) Lee, Y.; Huffman, C.; George, S. M. Selectivity in Thermal Atomic Layer Etching Using Sequential, Self Limiting Fluorination and Ligand-Exchange Reactions. *Chem. Mater.* **2016**, *28*, 7657–7665.

(36) Carver, C. T.; Plombon, J. J.; Romero, P. E.; Suri, S.; Tronic, T. A.; Turkot, R. B. Atomic Layer Etching: An Industry Perspective. *ECS J. Solid State Sci. Technol.* **2015**, *4*, N5005–N5009.

(37) Cano, A. M.; Lii-Rosales, A.; George, S. M. Thermal Atomic Layer Etching of Aluminum Nitride Using HF or XeF<sub>2</sub> for Fluorination and BCl<sub>3</sub> for Ligand Exchange. *J. Chem. Phys. C* **2022**, *126*, 6990–6999.

(38) Lemaire, P. C.; Parsons, G. N. Thermal Selective Vapor Etching of TiO<sub>2</sub>: Chemical Vapor Etching via WF<sub>6</sub> and Self-Limiting Atomic Layer Etching Using WF<sub>6</sub> and BCl<sub>3</sub>. *Chem. Mater.* **2017**, *29*, 6653–6665.

(39) Cano, A. M.; Natarajan, S. K.; Partridge, J. L.; Elliott, S. D.; George, S. M. Spontaneous Etching of B<sub>2</sub>O<sub>3</sub> by HF Gas Studied Using Infrared Spectroscopy, Mass Spectrometry, and Density Functional Theory. *J. Vac. Sci. Technol., A* **2022**, *40*, No. 022601.

(40) Mullins, R.; Natarajan, S. K.; Elliott, S. D.; Nolan, M. Self-Limiting Temperature Window for Thermal Atomic Layer Etching of HfO<sub>2</sub> and ZrO<sub>2</sub> Based on the Atomic-Scale Mechanism. *Chem. Mater.* **2020**, *32*, 3414–3426.

(41) Natarajan, S. K.; Cano, A. M.; Partridge, J. L.; George, S. M.; Elliott, S. D. Prediction and Validation of the Process Window for Atomic Layer Etching: HF Exposure on TiO<sub>2</sub>. *J. Phys. Chem. C* **2021**, *125*, 25589–25599.

(42) DuMont, J. W.; George, S. M. Pyrolysis of Alucone Molecular Layer Deposition Films Studied Using In Situ Transmission Fourier Transform Infrared Spectroscopy. *J. Phys. Chem. C* **2015**, *119*, 14603–14612.

(43) Ferguson, J. D.; Weimer, A. W.; George, S. M. Atomic Layer Deposition of Ultrathin and Conformal Al<sub>2</sub>O<sub>3</sub> Films on BN Particles. *Thin Solid Films* **2000**, *371*, 95–104.

(44) Ballinger, T. H.; Wong, J. C. S.; Yates, J. T. Transmission Infrared Spectroscopy of High Area Solid Surfaces - A Useful Method for Sample Preparation. *Langmuir* **1992**, *8*, 1676–1678.

(45) Lee, Y.; DuMont, J. W.; George, S. M. Atomic Layer Etching of  $\text{HfO}_2$  Using Sequential, Self-Limiting Thermal Reactions with  $\text{Sn}(\text{acac})_2$  and HF. *ECS J. Solid State Sci. Technol.* **2015**, *4*, N5013–N5022.

(46) Lee, Y.; Sun, H. X.; Young, M. J.; George, S. M. Atomic Layer Deposition of Metal Fluorides Using HF-Pyridine as the Fluorine Precursor. *Chem. Mater.* **2016**, *28*, 2022–2032.

(47) *HSC Chemistry*; HSC Chemistry 5.1, Outokumpu Research Oy: Pori, Finland.

(48) Deal, B. E.; Grove, A. S. General Relationship for Thermal Oxidation of Silicon. *J. Appl. Phys.* **1965**, *36*, 3770–3778.

(49) Gesenhues, U.; Wendt, H. True IE Mass Spectra of the Vapour Molecules of  $\text{AlCl}_3$  and  $\text{Al}_2\text{Cl}_6$ . *Int. J. Mass Spectrom. Ion Processes* **1986**, *70*, 225–229.

## Recommended by ACS

### Thermal Atomic Layer Etching of Aluminum Oxide ( $\text{Al}_2\text{O}_3$ ) Using Sequential Exposures of Niobium Pentafluoride ( $\text{NbF}_5$ ) and Carbon Tetrachloride ( $\text{CCl}_4$ ...

Varun Sharma, Mikko Ritala, *et al.*

APRIL 09, 2021  
CHEMISTRY OF MATERIALS

READ 

### Reaction Mechanisms of Non-hydrolytic Atomic Layer Deposition of $\text{Al}_2\text{O}_3$ with a Series of Alcohol Oxidants

Seunggi Seo, Bonggeun Shong, *et al.*

AUGUST 16, 2021  
THE JOURNAL OF PHYSICAL CHEMISTRY C

READ 

### $\text{AlO}_x$ Thin Films Synthesized by Mist Chemical Vapor Deposition, Monitored by a Fast-Scanning Mobility Particle Analyzer, and Applied as a Gate Insulating...

Arifuzzaman Rajib, Hajime Shirai, *et al.*

JANUARY 15, 2021  
ACS APPLIED ELECTRONIC MATERIALS

READ 

### Formation Mechanism of Self-Formed Triangular Pyramidal Patterns on Sapphire Substrate

Wei-Han Lai, Cheng-Yi Liu, *et al.*

JUNE 04, 2020  
CRYSTAL GROWTH & DESIGN

READ 

Get More Suggestions >